COMMUNICATION

Check for updates

A facile method for generating worm-like micelles with controlled lengths and narrow polydispersity†

Ouassef Nahi, [ID] *[a] Olivier J. Cayre,[a] Yi-Yeoun Kim, [ID] [b] Andrew J. Smith, [ID] [c] Nicholas J. Warren [ID] *[a] and Fiona C. Meldrum [ID] *[b]

This work shows that highly uniform worm micelles formed by polymerisation induced self-assembly can be obtained *via* simple post-synthesis sonication. Importantly, this straightforward and versatile strategy yields exceptionally monodisperse worms with tunable aspect ratios ranging from 7.2 to 17.6 by simply changing the sonication time.

Polymerisation-induced self-assembly (PISA) is a powerful and versatile strategy for forming block copolymer particles with controlled sizes and shapes.[1] Importantly, it is also industrially-relevant, where the production of nano-objects with solid contents of up to 50 wt% is readily scaled-up.[2] PISA is often used with controlled/living polymerisations,[1] where reversible addition–fragmentation chain transfer (RAFT) has the major advantage that it can be conducted using a wide range of functional monomers in aqueous[2] and organic media.[3] This gives rise to higher order polymeric architectures including spheres, worm-like micelles (worms) and vesicles. Of these, worms attract significant attention due to their flexibility, high surface areas and high aspect ratios, which are attractive for a wide range of applications, including viscosity modifiers,[4] drug delivery vectors,[5] and 3D cell growth/storage media.[6]

Although PISA provides precise control over many features of these nano-objects including the diameters of the spheres and vesicles, the thickness of the vesicle membrane,[7] and the cross-sectional diameter of worms,[8] it has proven extremely challenging to control the length and aspect ratios of the worms.[9] These constitute a transient phase between spheres and vesicles that often occupies a relatively narrow region of

phase space,[10] and reports of the production of worms with well-defined aspect ratios are rare.[11]

A very different strategy for controlling the dimensions of polymer worms – termed CDSA (crystallization-driven self-assembly) – was pioneered by Winnik and Manners.[12,13] In this method, ultrasound treatment of particles with crystalline core-forming blocks (typically poly(ferrocenylsilane) (PFS)) results in the formation of relatively short crystalline nano-fibers,[14] which then serve as "seeds" for the epitaxial growth of longer fibers through the condensation of soluble unimers.[15] This enables the formation of uniform cylindrical particles with tunable sizes, ranging from hundreds of nanometers up to a few microns.[14,15] However, this elegant CDSA method is restricted to a limited number of crystalline copolymers, and is a multi-step process conducted at low polymer concentrations. To overcome these limitations, a combined method using both PISA and CDSA (PI–CDSA) has recently emerged, where PISA was conducted with crystalline core-forming blocks, leading to the formation of high concentrations of well-defined block copolymer structures.[16] Nevertheless, reports of systems for which PI–CDSA can be performed remain rare and further understanding of the underlying mechanisms is still required.

This article describes a novel strategy for generating uniform copolymer worm particles with excellent control over their aspect ratios. It is both experimentally straightforward and versatile, and can potentially be applied to a wide range of copolymer worm systems. Taking inspiration from the CDSA seeding process, we show that the simple sonication of poly-disperse worms comprising poly(methacrylic acid)$_{70}$–poly(benzyl methacrylate)$_{100}$ (PMAA$_{70}$–PBzMA$_{100}$) yields well-defined worms with remarkable control over their lengths and dispersity. Evidenced by direct imaging and *in situ* SAXS measurements, this method holds enormous promise for a wide range of applications, where monodisperse, anisotropic nano-objects are required.[5,17]

PMAA$_{70}$–PBzMA$_{100}$ block copolymer worms were prepared *via* alcoholic RAFT dispersion polymerization as previously

[a] School of Chemical and Process Engineering, University of Leeds, Woodhouse Lane, Leeds, LS2 9JT, UK

[b] School of Chemistry, University of Leeds, Woodhouse Lane, Leeds, LS2 9JT, UK

[c] Diamond Light Source, Harwell Science and Innovation Campus, Harwell, Didcot, Oxfordshire, OX11 0DE, UK

† Electronic supplementary information (ESI) available: Experimental details including the synthesis of the worm block copolymers, sonication procedure, analytic methodologies, DLS analyses, GPC traces and additional SEM micrographs. See DOI: 10.1039/d0cc02313b
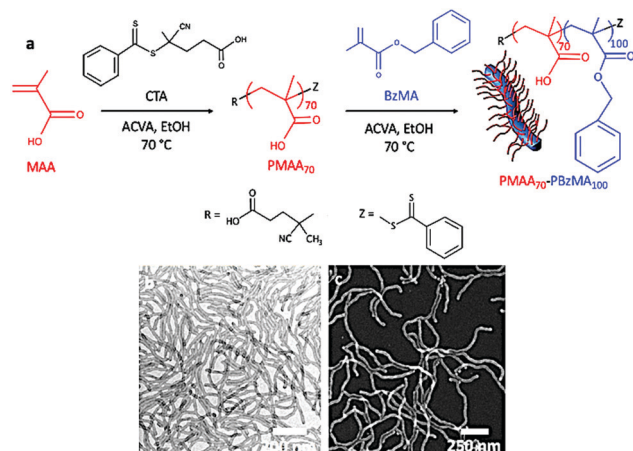
Fig. 1 (a) Synthesis of PMAA$_{70}$–PBzMA$_{100}$ worms *via* RAFT dispersion polymerisation in ethanol at 70 °C, mediated by PISA. (b) Transmission electron micrograph of the PMAA$_{70}$–PBzMA$_{100}$ worms (0.10 wt%). (c) Scanning electron micrograph of the worms.

Fig. 2 Scanning electron micrographs of the PMAA$_{70}$–PBzMA$_{100}$ worms (10 mg mL^{-1}) after sonication in an ice bath for (a) 0 min, (b) 1 min, (c) 5 min, and (d) 15 min.

reported by Armes *et al.*[18] First, a dithiocarbonate-based chain-transfer agent (CTA) was used to polymerize methacrylic acid and form the poly(methacrylic acid) (PMAA$_{70}$) macro-CTA, with a mean degree of polymerisation (DP) of 70 (as determined by ^{1}H NMR). After purification, this homopolymer was chain-extended with benzyl methacrylate (BzMA) in ethanol to produce the targeted diblock copolymer with a mean DP for the PBzMA block of 100. During the process, the PMAA$_{70}$–PBzMA$_{100}$ chains underwent *in situ* self-assembly to form block copolymer worms (Fig. 1a). Gel permeation chromatography (GPC) analysis in THF (Fig. S1, ESI†) indicated a narrow molar mass distribution for both the PMAA macro-CTA ($M_n \approx 13\,500$ g mol^{-1}, $M_w \approx 14\,700$ g mol^{-1}, $M_w/M_n \approx 1.09$) and the PMAA$_{70}$–PBzMA$_{100}$ diblock copolymer ($M_n \approx 29\,600$ g mol^{-1}, $M_w \approx 33\,300$ g mol^{-1}, $M_w/M_n \approx 1.12$). However, the GPC trace of the PMAA$_{70}$–PBzMA$_{100}$ copolymer shows a shoulder at low molecular weight. This was attributed to some contamination resulting from the exhaustive methylation of the PMAA residues carried out to render the copolymer soluble in THF.[19]

Post mortem transmission electron microscopy (TEM) was used to characterize the block copolymer worms after staining the dried samples with uranyl acetate (Fig. 1b). The worms were present as a pure phase, but were highly polydisperse, with lengths ranging from 300 nm up to 3 μm. This large range is typical of PISA[9] and significantly limits the use of polymer worms in many applications.[17] We also used scanning electron microscopy (SEM) to characterize these polymer nano-objects and observed comparable structures (Fig. 1c and 2a). With no stain required, its simplicity in operation, and arguably superior images, SEM was used extensively to characterize the worms in these experiments. To induce worm scission, ethanolic solutions of the PMAA$_{70}$–PBzMA$_{100}$ worms (10 mg mL^{-1} and 100 mg mL^{-1}) were gently ultrasonicated for an hour (using an ultrasonic probe Fisherbrand™ Q125 Sonicator – 120 Watts, operating at 10% amplitude) and aliquots were collected at various time intervals for characterization. The samples were immersed in an ice bath throughout to maintain a temperature
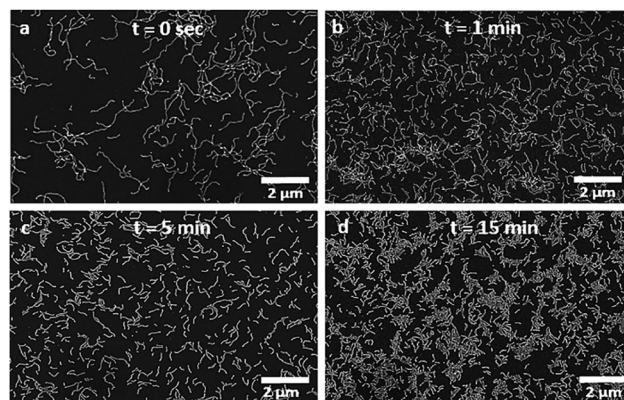
close to 0 °C, thereby preventing any temperature-induced change in morphology. The SEM micrographs demonstrate that the worm particles experience rapid and progressive fragmentation under the shear stress induced by ultrasonication (Fig. 2 and Fig. S2, ESI†). As shown in Fig. 2, a dramatic reduction in the worm length occurs within 5 min of mild sonication, and little further change occurs after 10 min. This was also confirmed by the dynamic light scattering (DLS) analyses of the sonicated worms (Fig. S4, ESI†).

The impact of sonication on the worms was quantified by determining the number-average length (L_n), the weight-average length (L_w) and the polydispersity index (PDI) of the worms at various sonication times and copolymer concentrations, as obtained from the SEM micrographs (Table S1, ESI†). At both copolymer concentrations investigated (10 mg mL^{-1} and 100 mg mL^{-1}), splitting of the worms yielded shorter and more uniform particles. Indeed, a dramatic shortening of the worms from $L_n \approx 1.5$ μm to $L_n \approx 420$ nm was observed after only 30 seconds of mild sonication, corresponding to a reduction of about 72% of the length of the worms (Fig. 3). Additionally, after 1 h of sonication, the as-synthesized polydisperse worms ($L_n = 1450$ nm, $L_w = 3125$ nm, PDI = 2.15) fragmented into shorter and significantly more monodisperse worms ($L_n = 247$ nm, $L_w = 256$ nm, PDI = 1.03). This demonstrates that it is possible to generate highly uniform worms with tunable aspect ratios by simply varying the sonication time (Table S1, ESI†).

Interestingly, shorter particles ($L_n = 179$ nm, $L_w = 211$ nm, PDI = 1.18) were achieved on prolonged sonication of low worm concentrations (10 mg mL^{-1}) as compared with higher concentrations (100 mg mL^{-1}, $L_n = 247$ nm, $L_w = 256$ nm, PDI = 1.03). The worm length also "plateaus" at a lower value of $L_n = 179$ nm for the 10 mg mL^{-1} sample as compared with $L_n = 247$ nm for the 100 mg mL^{-1} sample. This can be attributed to the increase in solution viscosity that accompanies an increase in the copolymer concentration. Higher viscosities are expected to impede the formation of cavitation bubbles, and thus reduce the efficiency of worm splitting.[20] Nevertheless, for both copolymer concentrations, sonication enabled the aspect ratio of the worms to be tuned from 7.2 to 17.6 with narrow length dispersity, as shown by the reduction in contour length and polydispersity (Fig. 3 and Table S1, ESI†).
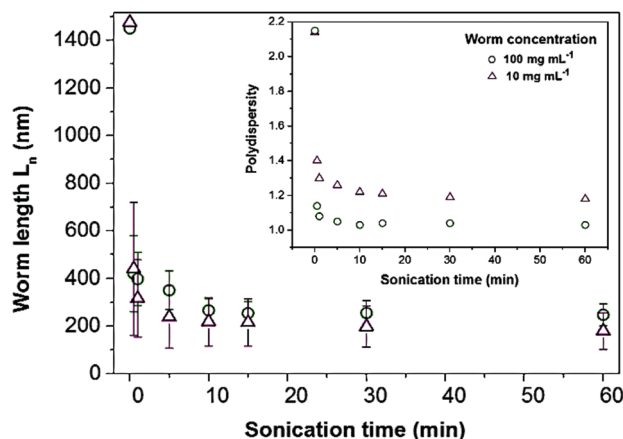
Fig. 3 Number-average length (L_n) and polydispersity of the PMAA$_{70}$–PBzMA$_{100}$ worms as a function of sonication time for polymer concentrations of 10 mg mL^{-1} (purple triangles) and 100 mg mL^{-1} (green circles), as derived from analysis of the SEM images. The error bars represent the standard deviations of the measured worm lengths. The large error bar ($\approx$1 μm, resulting from the polydispersity of the as-synthesized objects) for the non-sonicated worms (t = 0 min) is not shown for the sake of clarity.

It is also emphasized that the short worm particles exhibit considerable stability, where negligible changes in the morphology, size and polydispersity of the shorter worms were observed after three months.

These findings were also supported by synchrotron small-angle X-ray scattering (SAXS) measurements, which enabled the splitting process to be monitored *in situ* (Fig. 4). This technique is extremely powerful as the data is averaged from millions of particles; it therefore records the worm dimensions in solution without the artefacts that can arise during sample preparation for electron microscopy. Experiments were conducted with 10 mg mL^{-1} solutions, where the SAXS pattern for the non-sonicated worms exhibited a low q gradient of −1 and could be accurately fitted to a single cylindrical micelle model.[21] This is fully consistent with the worm morphology observed in electron microscopy (Fig. 1b, c and 2). The mean contour length of the worms (L_c), the radius of

the core-forming block (PBzMA) and the radius of gyration of the worm corona (PMAA) extracted from the fittings performed are summarized in Table S2 (ESI†).

Upon sonication, the aspect ratio of the worms undergoes a monotonic decrease, as shown by the deviation of the gradient in the low q region (0.02 nm^{-1} < q < 0.10 nm^{-1}) from −1 towards 0 (Fig. 4). In order to determine precise dimensions, a combination of a cylindrical and spherical micelle model was first applied but did not give a satisfactory fit. This indicates that the sample principally comprises worms, as is consistent with the SEM images (Fig. S2, ESI†). The formation of spheres would also be indicated by a characteristic zero gradient in the low q regime.[22] This further demonstrates that the shear stress resulting from the sonication is insufficient to induce a phase transformation of the worms. At long sonication times, a satisfactory fit was achieved using a combination of Gaussian chain and cylindrical micelle models.[23] This suggests that extensive sonication induces minor dissolution of polymer chains into the bulk solution.

In common with the SEM study, the SAXS data show that the splitting rate is highest in the first few minutes of sonication. This is due to the higher tensile stress experienced by the longer worms. It then significantly decreases, reaching L_n ≈ 200 nm after 10 min of sonication, corresponding to a worm length reduction of approximately 86% (Fig. 4b). The splitting process then continues beyond this point, but at a significantly slower rate. This suggests a critical worm length for which the shear stress generated by sonication is insufficient to generate further splitting. The local minimum at q ≈ 0.3 nm^{-1} shows that the mean worm width remains constant at R_{core} = 10.4 ± 2.0 nm throughout the sonication process. A slight increase in the dispersity of the cores (from 10.2% to 14.1%) and a small decrease in the radius of gyration of the worm corona (from 2.8 nm to 2.1 nm) is also observed (Fig. 4b and Table S2, ESI†). This is indicative of minor release of free polymer from the worms on extended sonication, as supported by GPC analyses (Fig. S1, ESI†); a small shoulder at low molecular weight appears after an hour of sonication (*i.e.*, far beyond the point at which this synthetic method would be terminated in practice).
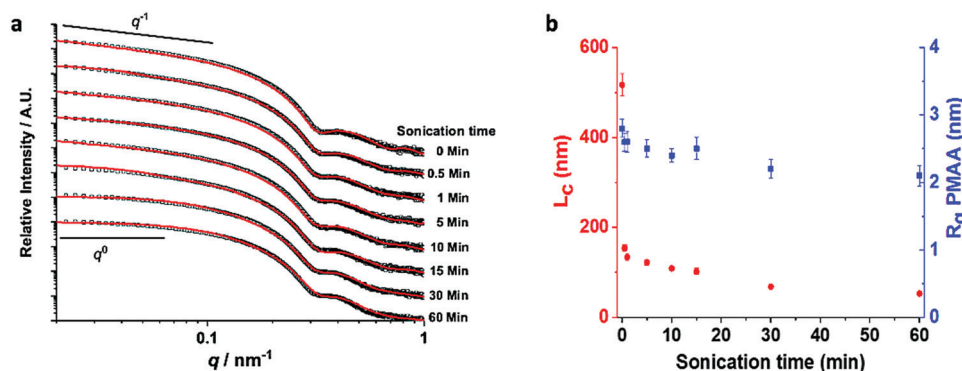

Fig. 4 (a) Representative SAXS patterns acquired *in situ* of an ethanolic dispersion of PMAA$_{70}$–PBzMA$_{100}$ (10 mg mL^{-1}) particles sonicated over time. The black squares represent the experimental data collected, while the solid red lines correspond to the best data fits obtained by a combination of cylindrical and spherical fitting models. The gradients of −1 and 0 in the low q region are shown as a guide to the eye. (b) Corresponding mean contour length of the worms (L_c; red dots) and radius of gyration of the worm corona (R_g PMAA; blue squares) as a function of sonication time. The error bars represent the average error to the fitting.

The mechanism of worm splitting is intriguing and is likely to be analogous to the CDSA fragmentation process.[12,13] Sonication causes cavitation, where implosion of gas bubbles creates a solvodynamic shear field gradient that is maximal at the vicinity of the collapsing cavity.[24] Worm segments in close proximity to a bubble experience intense shear as they are pulled towards the center of the cavity. This generates a velocity gradient along the long axis of the worms that is counter-balanced by the mechanical tensile strength of the worms.[24] When the shear stress reaches a critical level, the worms are pulled apart and split preferentially along their long axis, as indicated by the reduction of the worm length upon sonication without significant alteration of their diameters (Fig. 4 and Table S2, ESI†). That the splitting events level-off upon prolonged sonication is attributed to the stress forces that scale with the length of the worms.[24] Therefore, when the worms reach a critical value (*i.e.*, $L_n \approx 200$ nm), the shear stress becomes insufficient to induce further splitting.

Finally, the versatility of our strategy was demonstrated by using it to control the dimensions of worms of a second block copolymer, poly(glycerol monomethacrylate)$_{53}$–poly(2-hydroxypropyl methacrylate)$_{110}$ (PGMA$_{53}$–PHPMA$_{110}$). This copolymer was selected as it dissociates into unimers when submitted to high shear homogenization.[2] This is due to the weakly hydrophobic PHPMA core-forming block that limits its ability to retain the worm morphology under shear stress. Chemical cross-linking of PGMA$_{53}$–PHPMA$_{110}$ worms using ethylene glycol dimethacrylate enhances the cohesion between the polymer molecules and enables them to survive sonication. Cross-linked PGMA$_{53}$–PHPMA$_{110}$ was therefore synthesized using RAFT mediated-PISA,[10] and formed worms (Fig. S6, ESI†). Importantly, an identical pattern of results was obtained with this polymer, where sonication again yielded shorter worms with narrower size distributions (Fig. S6, ESI†).

In summary, this study demonstrates that it is possible to tune the length of worm micelles produced by RAFT-mediated PISA by simple post-polymerisation ultrasonication. This straightforward and versatile method circumvents the need to synthesize particles under stringent conditions to obtain worm nano-objects with specific sizes and can be applied to copolymers that do not possess a crystalline core-forming block. Our approach is expected to be transferable to other polymeric nano-objects, provided that the core-forming block is sufficiently robust to retain the anisotropic morphology. The ability to exert dimensional control over worm micelles, combined with the scalability potential of PISA, offers new opportunities to expand their array of applications, where uniform anisotropic structures hold great promise.

Conflicts of interest

There are no conflicts to declare.

References

1 S. Brusseau, F. Dagosto, S. Magnet, L. Couvreur, C. Chamignon and B. Charleux, *Macromolecules*, 2011, **44**, 5590–5598.
2 N. J. Warren and S. P. Armes, *J. Am. Chem. Soc.*, 2014, **136**, 10174–10185.
3 M. Semsarilar, E. R. Jones, A. Blanazs and S. P. Armes, *Adv. Mater.*, 2012, **24**, 3378–3382.
4 Y. S. Thio, J. Wu and F. S. Bates, *Macromolecules*, 2006, **39**, 7187–7189.
5 Y. Geng, P. Dalhaimer, S. Cai, R. Tsai, M. Tewari, T. Minko and D. E. Discher, *Nat. Nanotechnol.*, 2007, **2**, 249–255.
6 I. Canton, N. J. Warren, A. Chahal, K. Amps, A. Wood, R. Weightman, E. Wang, H. Moore and S. P. Armes, *ACS Cent. Sci.*, 2016, **2**, 65–74.
7 C. Gonzato, M. Semsarilar, E. R. Jones, F. Li, G. J. P. Krooshof, P. Wyman, O. O. Mykhaylyk, R. Tuinier and S. P. Armes, *J. Am. Chem. Soc.*, 2014, **136**, 11100–11106.
8 N. J. Warren, M. J. Derry, O. O. Mykhaylyk, J. R. Lovett, L. P. D. Ratcliffe, V. Ladmiral, A. Blanazs, L. A. Fielding and S. P. Armes, *Macromolecules*, 2018, **51**, 8357–8371.
9 A. Blanazs, R. Verber, O. O. Mykhaylyk, A. J. Ryan, J. Z. Heath, C. W. I. Douglas and S. P. Armes, *J. Am. Chem. Soc.*, 2012, **134**, 9741–9748.
10 A. Blanazs, A. J. Ryan and S. P. Armes, *Macromolecules*, 2012, **45**, 5099–5107.
11 C. A. Figg, R. N. Carmean, K. C. Bentz, S. Mukherjee, D. A. Savin and B. S. Sumerlin, *Macromolecules*, 2017, **50**, 935–943.
12 G. Guérin, H. Wang, I. Manners and M. A. Winnik, *J. Am. Chem. Soc.*, 2008, **130**, 14763–14771.
13 X. Wang, G. Guerin, H. Wang, Y. Wang, I. Manners and M. A. Winnik, *Science*, 2007, **317**, 644–647.
14 J. Qian, Y. Lu, G. Cambridge, G. Guérin, I. Manners and M. A. Winnik, *Macromolecules*, 2012, **45**, 8363–8372.
15 H. Qiu, Y. Gao, V. A. Du, R. Harniman, M. A. Winnik and I. Manners, *J. Am. Chem. Soc.*, 2015, **137**, 2375–2385.
16 C. E. Boott, J. Gwyther, R. L. Harniman, D. W. Hayward and I. Manners, *Nat. Chem.*, 2017, **9**, 785–792.
17 S. Kaga, N. P. Truong, L. Esser, D. Senyschyn, A. Sanyal, R. Sanyal, J. F. Quinn, T. P. Davis, L. M. Kaminskas and M. R. Whittaker, *Biomacromolecules*, 2017, **18**, 3963–3970.
18 S. P. Semsarilar, M. Ladmiral, V. Blanazs and A. Armes, *Polym. Chem.*, 2014, **5**, 3466–3475.
19 A. A. Cockram, T. J. Neal, M. J. Derry, O. O. Mykhaylyk, N. S. J. Williams, M. W. Murray, S. N. Emmett and S. P. Armes, *Macromolecules*, 2016, **50**, 796–802.
20 M. M. Caruso, D. A. Davis, Q. Shen, S. A. Odom, N. R. Sottos, S. R. White and J. S. Moore, *Chem. Rev.*, 2009, **109**, 5755–5798.
21 S. P. Derry, M. J. Mykhaylyk and O. O. Armes, *Angew. Chem., Int. Ed.*, 2017, **129**, 1–6.
22 V. J. Cunningham, A. Blanazs, N. J. Warren, A. J. Smith, O. O. Mykhaylyk and S. P. Armes, *J. Am. Chem. Soc.*, 2014, **136**, 6307–6317.
23 M. K. Kocik, O. O. Mykhaylyk and S. P. Armes, *Soft Matter*, 2014, **10**, 3984–3992.
24 Y. Y. Huang, T. P. J. Knowles and E. M. Terentjev, *Adv. Mater.*, 2009, **21**, 3945–3948.